PCCP

Surface Anchored Self-Assembled Reaction Centre Mimics as Photoanodes Consisting of a Secondary Electron Donor, Aluminium(III) Porphyrin and TiO2 Semiconductor

Journal:	*Physical Chemistry Chemical Physics*
Manuscript ID	CP-ART-06-2019-003400.R1
Article Type:	Paper
Date Submitted by the Author:	02-Aug-2019
Complete List of Authors:	Zarrabi, Niloofar; University of Minnesota Duluth Lim, Gary; UNT, Chemistry Bayard, Brandon; University of Minnesota Duluth, aDepartment of Chemistry & Biochemistry D'Souza, Francis; University of North Texas, Chemistry Poddutoori, Prashanth; University of Minnesota Duluth, Chemistry&Biochemistry

ARTICLE

Surface Anchored Self-Assembled Reaction Centre Mimics as Photoanodes Consisting of a Secondary Electron Donor, Aluminium(III) Porphyrin and TiO_2 Semiconductor†

Received 00th January 20xx,
Accepted 00th January 20xx

DOI: 10.1039/x0xx00000x

NIloofar Zarrabi,[a] Gary N. Lim,[b] Brandon J. Bayard,[a] Francis D'Souza,*[,b] and Prashanth K. Poddutoori*[,a]

A series of vertically assembled photoanodes, consisting of 5,10,15,20-tetrakis(3,4,5-trifluorophenyl)aluminum(III) porphyrin ($AlPorF_3$), pyridine appended electron donor (PTZ-Py, PTZ = phenothiazine; TTF-Py, TTF = tetrathiafulvalene), and semiconductor TiO_2, have been fabricated by exploiting the unique axial properties of $AlPorF_3$. The new photoanodes were characterized by steady-state and transient spectroscopic techniques. Transient-absorption studies show that in the absence of donor, both the photoanodes ($AlPorF_3$-TiO_2 and $AlPorF_3$-Ph-TiO_2) exhibit electron injection from $AlPorF_3$ to the conduction band of TiO_2 and the injection efficiencies are strongly dependent on the linker. Faster electron injection and recombination is revealed when the $AlPorF_3$ is directly bound to the TiO_2. While a secondary electron donor is coordinated to $AlPorF_3$, (viz., Donor-Py-$AlPorF_3$-TiO_2 and Donor-Py-$AlPorF_3$-Ph-TiO_2) the primary charge separation occurs in the form of electron injection from the $AlPorF_3$ to TiO_2 followed by a secondary process involving photooxidation of the donor (PTZ, TTF) with $AlPorF_3^{\bullet+}$ is revealed. The estimated electron injection lifetimes and the $AlPorF_3^{\bullet+}$ decay lifetimes strongly depend on electron richness of the donor, the higher the electron density on the donor, the faster the electron injection and photooxidation are witnessed. The photoanodes with TTF (TTF-Py-$AlPorF_3$-TiO_2 and TTF-Py-$AlPorF_3$-Ph-TiO_2) shows faster injection and shorter decay lifetimes of $AlPorF_3^{\bullet+}$ over its PTZ counterparts (PTZ-Py-$AlPorF_3$-TiO_2 and PTZ-Py-$AlPorF_3$-Ph-TiO_2). The observed trends suggest that the strong secondary electron donor enhances the injection and the subsequent photooxidation processes in the investigated photoanodes. The successful mimicking of a sequential charge-separation process makes aluminum(III) porphyrins potential sensitizers for construction of photoanodes, especially for photocatalytic and dye-sensitized solar cells for conversion and storage of solar energy.

1. Introduction

Mimicking of photosynthesis is one of the successful strategies for tapping the sunlight energy into electricity or chemical energy.[1-10] The solar energy conversion in photosynthesis is achieved by a multi-step electron transfer reaction in which the initial charge separation is stabilized by a series of sequential electron transfer steps by moving the charges further part. As a result, a long-lived charge-separated state with high quantum yield is produced.[11-14] The resulting charge-separated state consists of photon energy in the form of potential energy, which ultimately utilized in performing nature's two fundamental reactions, viz., production of chemical energy, that is, the reduction of carbon dioxide to carbohydrates, and oxidation of water to oxygen gas and protons. This overall process can be projected as a light-driven electrochemical cell in which the anodic reaction extracts electrons from water, releasing protons and oxygen, while the cathodic reaction reduces protons, carbon dioxide, or some other species to generate fuel energy carriers. Several recent studies have explored dye-sensitized metal oxide semiconductors as anodes for such photoelectrochemical cells.[3, 8-10, 15-18] Among the challenges in designing such a system is simultaneously achieving a high quantum yield of electron injection into the semiconductor and long-lived charge separation while generating sufficient oxidizing potential for catalytically withdrawing electrons from water.

To model these processes, many elegant photoanodes have been designed and synthesized. Within these model compounds, porphyrin derivatives are widely used as photosensitizers because they are redox-tuneable and absorb strongly in the visible light region of the solar spectrum.[7, 8, 16-22] However, for a large extent, transition metal ion based porphyrin derivatives were used and, a very little attention was paid towards the main group element porphyrin (MGP) derivatives.[20, 21, 23] Among the porphyrins, MGPs are unique as their redox potentials are tuned by central element in its cavity, which in principle bypass the complicated synthetic methods to

[a]*Department of Chemistry & Biochemistry, 1038 University Drive, University of Minnesota Duluth, Duluth, MN, 55812, USA. Email: ppk@d.umn.edu*
[b]*Department of Chemistry, University of North Texas, 1155 Union Circle, #305070, Denton, TX 76203-5017, USA. E-mail: Francis.DSouza@UNT.edu*

†Electronic Supplementary Information (ESI) available: ^1H NMR spectra, electrochemistry of PTZ-Py, transient absorption spectra of $AlPorF_3$-OH and $AlPorF_3$-Ph-HMAH, and the spectroelectrochemical data of PTZ-Py, TTF-Py and $AlPorF_3$-Ph. [details of any supplementary information available should be included here]. See DOI: 10.1039/x0xx00000x

accomplish the required redox potentials for the desired application. By insertion of main-group elements with different oxidation states results in a broad range of redox potentials. For example, upon insertion of Al(III) ion in tetratolylporphyrin (TTP) results in potentials that are moderate and are the best fit for construction of reaction centre complex,[24-30] whereas insertion of P(V) in the same TTP results high-potential porphyrin with the redox potentials desirable for the construction of photoanode.[31] Moreover, MGPs can form axial bonds that allow two molecular components to be attached. By exploiting these properties, we and others reported several model compounds for reaction centre complex and photoanodes, which are derived from aluminum(III) porphyrin (AlPor) and phosphorus(V) porphyrin (PPor) derivatives.[20, 23-38] AlPors react with carboxylic acids to form covalent ester linkages, whereas Lewis bases, such as pyridine and imidazole, form coordination bonds to the Al centre, which is a Lewis acid. The combination of optical, redox and structural properties makes AlPor an ideal candidate for constructing multi-component D–A systems in which the electron-transfer pathway is perpendicular to the porphyrin plane. For this purpose, we utilized well know 2D and 3D electron acceptors. More recently, we replaced these traditional electron acceptors with semiconductor nanoparticles such as TiO_2 to build a multi-modular photoanodes.[21] Here TiO_2 plays a dual role, it not only provides the support for surface anchoring but also it induces the primary charge separation between porphyrin and conduction band, which subsequently results in the photooxidation of the donor. One advantage of such an arrangement is that the donor and acceptor sides of the complex are located on opposite faces of the porphyrin, which maximizes the spatial separation of the charges produced by the electron transfer. Moreover, the π^* orbital of the porphyrin resides in the same region of space as the axial ligands, which should increase the electronic coupling between the excited state of the porphyrin and the acceptor and, hence, promote electron transfer. Together with these advantages, it could be feasible to address the challenges in designing photoanodes such as achieving a high quantum yield of electron injection into the semiconductor with long-lived charge separation and producing high oxidation potentials for catalytic reactions.

In continuation to our effort to understand the intricate details here, we report a series of new photoanodes comprised of high-potential aluminium(III) porphyrin ($AlPorF_3$), a secondary electron donor (= PTZ-Py, TTF-Py) and wide bandgap semiconductor TiO_2 with the general formula 'Donor-Py-$AlPorF_3$-TiO_2' and 'Donor-Py-$AlPorF_3$-Ph-TiO_2'. The surface of the particles is covered with a layer of $AlPorF_3$ molecules that absorb light and inject electrons into the semiconductor. The oxidized dye ($AlPorF_3^{\bullet+}$) is regenerated through reduction by a secondary electron donor. The electron injection and photooxidation process are easily detected by transient absorption spectroscopy. Using this technique, the kinetics of the electron transfer are evaluated. We have studied the dependence of these properties on the porphyrin–TiO_2 distance by varying the bridge between $AlPorF_3$ and TiO_2, and we show that the injection and recombination are strongly reliant on the distance. We find spectroscopic evidence of electron injection from the photo-excited $AlPorF_3$ into the conduction band of TiO_2, followed by secondary electron transfer from donor (PTZ/TTF) to the oxidized porphyrin, $AlPorF_3^{\bullet+}$. The ability of the molecular assembly to photo-oxidize the donor suggests that the studied design principle could be a promising way to construct photoanodes for water oxidation.

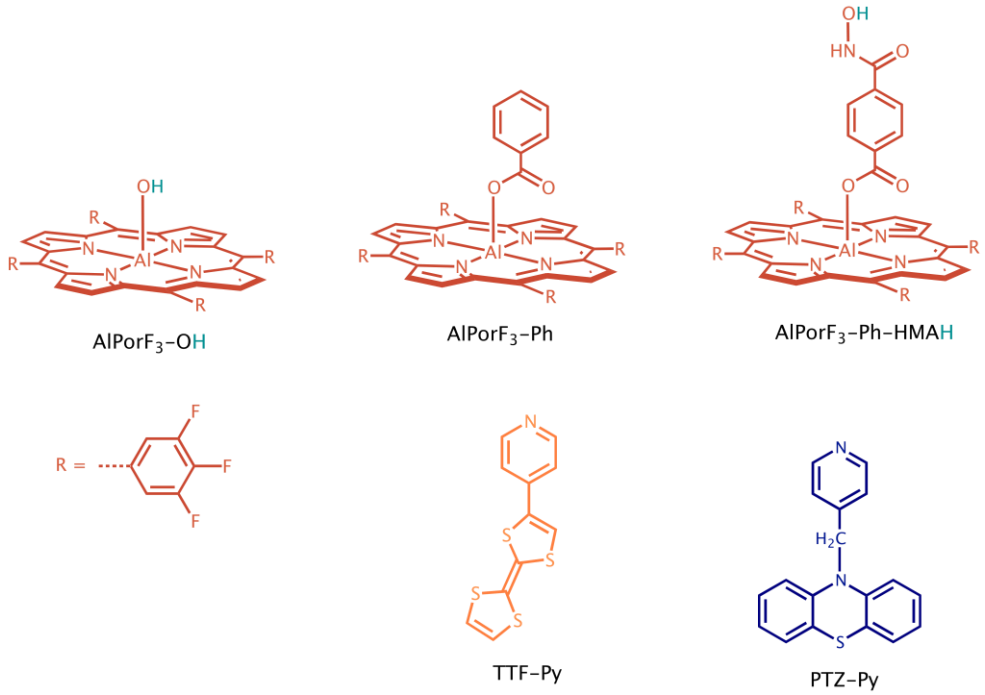

Chart 1. Structural information of the investigated compounds.

ARTICLE

2. Experimental section

2.1 Synthesis. All the chemicals, solvents and chromatographic materials were obtained from Aldrich Chemicals and were used as received. The TiO_2 (Aeroxide P25) were obtained from Evonik Industries. Synthesis of the investigated porphyrin derivatives ($AlPorF_3$-Ph-HMAH, $AlPorF_3$-Ph, and $AlPorF_3$-OH)[21], and non-porphyrinic electron donors (PTZ-Py and TTF-Py)[27, 28] were reported elsewhere, Chart 1.

3. Physical methods

3.1 Absorption and fluorescence titrations. The UV/Vis titrations were recorded with an Agilent Cary 100 UV-VIS spectrometer. Steady-state fluorescence titrations were recorded using a Photon Technologies International Quanta Master 8075-11 spectrofluorimeter, equipped with a 75 W xenon lamp, running with FelixGX software. Titrations were carried out in CH_2Cl_2 at concentrations appropriate for measuring the porphyrin Q band. A solution containing $AlPorF_3$-Ph was placed in a cuvette and titrated by adding aliquots of a concentrated solution of the donor (PTZ-Py or TTF-Py). The donor solution also contained the $AlPorF_3$-Ph at its initial concentration so that the porphyrin concentration remained constant throughout the titration. The binding constants were calculated by fitting the equation[21, 39]

$$\Delta A_{598} = \frac{\varepsilon}{2}\left[\left([AlPorF_3] + [D] + \frac{1}{K}\right) - \sqrt{\left([AlPorF_3] + [D] + \frac{1}{K}\right)^2 - 4[AlPorF_3][D]}\right] \quad (1),$$

where ΔA_{598} is the absorbance change at 598 nm. [$AlPorF_3$] is the total concentration of bound and unbound acceptor and is kept fixed, Abs is the absorption of complex at the wavelength λ, [D] is the total concentration of the donor which is varied, K is binding constant and ε is the molar absorptivity of PTZ-Py-$AlPorF_3$-Ph or TTF-Py-$AlPorF_3$-Ph complex. In an analogous manner, steady-state fluorescence titrations were carried out using solutions at a constant concentration of $AlPorF_3$-Ph and varying concentration of donor. The solutions were excited at the isosbestic point wavelength, which was obtained from the corresponding absorption titrations.

3.2 Preparation of thin films of dye-sensitized TiO_2. TiO_2 nanoparticles (Aeroxide P25) were mixed into a paste by combining 1.0 g of dry nanoparticles with 2 ml of H_2O and 2 mL of C_2H_5OH. The paste was then doctor-bladed onto 1 mm thick fused silica microscope slides (1 x 1 in, GM Associates). The resulting films were then sintered in air at 450°C for two hours. The anchor-bound photoanodes ($AlPorF_3$-Ph-TiO_2) prepared by soaking the bare semiconductor films for 12 h in a 0.1 mM solution of $AlPorF_3$-Ph-HMAH in CH_2Cl_2 containing few drops of methanol. The directly bound photoanodes ($AlPorF_3$-TiO_2) were prepared by soaking the films in a 0.1 mM solution of $AlPorF_3$-OH in benzene at 80°C for 12h. The same sensitized films were also used to collect absorption spectra of the dye on the semiconductor surface.

3.3 Femtosecond Transient Absorption Spectroscopy. Femtosecond transient absorption spectroscopy experiments were performed using an Ultrafast Femtosecond Laser Source (Libra) by Coherent incorporating a diode-pumped, mode-locked Ti:Sapphire laser(Vitesse) and diode-pumped intracavity doubled Nd:YLF laser (Evolution) to generate a compressed laser output of 1.45 W. For optical detection, a Helios transient absorption spectrometer coupled with a femtosecond harmonics generator, both provided by Ultrafast Systems LLC, was used. The source for the pump and probe pulses was derived from the fundamental output of Libra (compressed output 1.45 W, pulse width 90 fs) at a repetition rate of 1 kHz. 95% of the fundamental output of the laser was introduced into a harmonic generator which produced second and third harmonics of 400 and 267 nm besides the fundamental 800 nm for excitation, while the rest of the output was used for generation of the white light continuum. In the present study, the second harmonic 400 nm excitation pump was used in all the experiments. Kinetic traces at appropriate wavelengths were assembled from the time- resolved spectral data. Data analysis was performed using Surface Xplorer software supplied by Ultrafast Systems.

4. Results and discussion

4.1 Characterization of the self-assembled dyads. Scheme 1 shows the formation of the investigated self-assembled dyads. Figure S1 shows the ^{1}H NMR spectrum of a 1:1 mixture of $AlPorF_3$-Ph and PTZ-Py (bottom) along with the individual spectra of $AlPorF_3$-Ph (top) and PTZ-Py (middle). In the coordination complex, shielding due to the porphyrin ring

ARTICLE

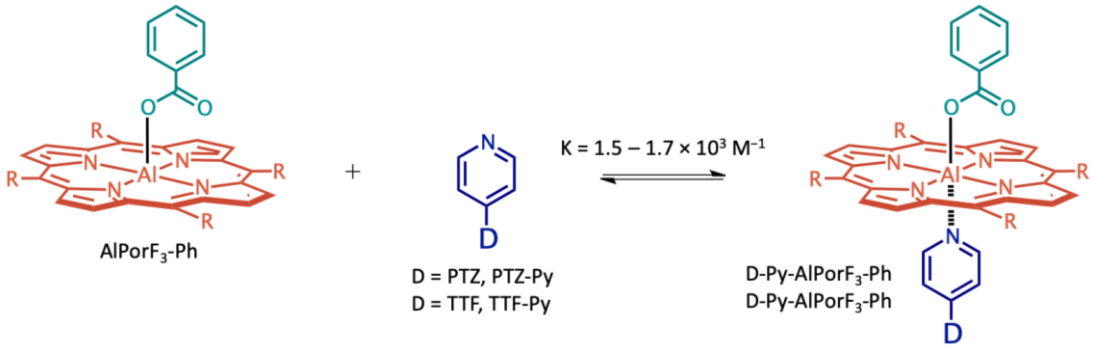

Scheme 1. Scheme represents the formation of the dyads Donor–Py–AlPorF$_3$–Ph in CH_2Cl_2. Donor = PTZ, TTF.

causes an upfield shift of the PTZ-Py protons on the pyridine unit (from 8.55 and 7.30 to 6.48 and 6.15 ppm), bridging methylene group (from 5.08 ppm to 4.65 ppm) as indicated by the dashed lines. The magnitude of the shift depends on the distance of the protons from the porphyrin ring, and the pyridinyl protons display the greatest shift indicating that coordination occurs via the pyridinyl group. On the benzoate

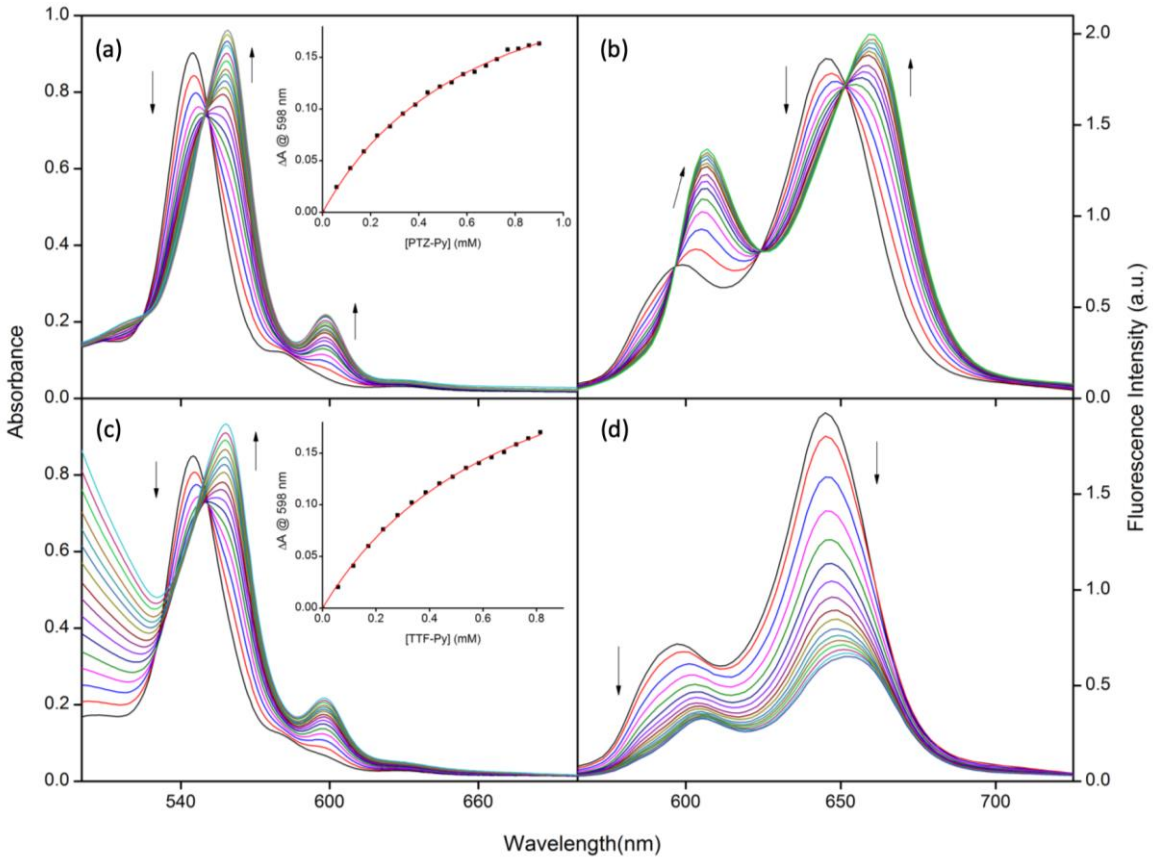

Figure 1. (a) Absorption and (b) fluorescence titrations of AlPorF$_3$-Ph with PTZ-Py; and (c) absorption and (d) fluorescence titration of AlPorF$_3$-Ph with TTF-Py in CH_2Cl_2. The inset shows a plot of the change of absorbance at 598 nm and the fit for the formation of a 1:1 complex. PTZ-Py or TTF-Py was added up to 8.14×10^{-4} M or 9.83×10^{-3} M, respectively, in 10 µL (5.90×10^{-3} M) increments to 1 mL (6×10^{-5} M) solution of AlPorF$_3$-Ph. The excitation wavelength was chosen at the isosbestic point, 550 nm, which was obtained from absorption titrations.

ARTICLE

group, the protons closest to the porphyrin ring show an increased upfield shift upon coordination, 4.95 ppm to 4.77 ppm, suggesting that the aluminium(III) centre lies out of the porphyrin plane in $AlPorF_3$-Ph and is pulled into the plane when PTZ-Py coordinates. Similar results were obtained for complexation of $AlPorF_3$-Ph with TTF-Py, see Figure S2.

The particulars of steady-state absorption spectra of investigated compounds are described elsewhere.[21] Briefly, the absorption spectra of the $AlPorF_3$-Ph-HMAH and $AlPorF_3$-Ph are very similar in spectral shapes and molar extinction coefficients suggesting that the electronic structure of the $AlPorF_3$ is not perturbed by the axial phenyl unit. Figure 1a shows spectral titrations of $AlPorF_3$-Ph with PTZ-Py in CH_2Cl_2. Upon addition of PTZ-Py, the Q-bands of the porphyrin shift from 544 and 559 nm to 581 and 598 nm. An isosbestic point is observed at 550 nm, indicating complex formation. The observed shifts in the porphyrin bands are typical of axial coordination of nitrogen ligands to $AlPorF_3$.[24, 25, 27-30] Analysis of the data using equation 1[39] gives a plot (Figure 1a, inset) confirming the 1:1 complex formation and the slope yields the binding constant (K) of 1.7×10^3 M^{-1}. Similar spectral changes and binding constants were observed in titrations of $AlPorF_3$-Ph *vs* TTF-Py ($K = 1.5 \times 10^3$ M^{-1}), see Figure 1c. The absence of any additional bands in these titrations suggests that perturbation of the electronic structures of the photo- and redox-active components due to formation of the complex is relatively small. Together with the NMR, absorption, and fluorescence titrations, we conclude the formation of the TTF-Py-$AlPorF_3$-Ph and PTZ-Py-$AlPorF_3$-Ph in solution.

4.2 Fabrication of photoanodes. The $AlPorF_3$ was anchored on the TiO_2 in two different modes: (i) through an ether linker and (ii) through the phenyl hydroxamate linker. These two different binding modes enable to study the electron injection kinetics as a function of the distance between $AlPorF_3$ and the

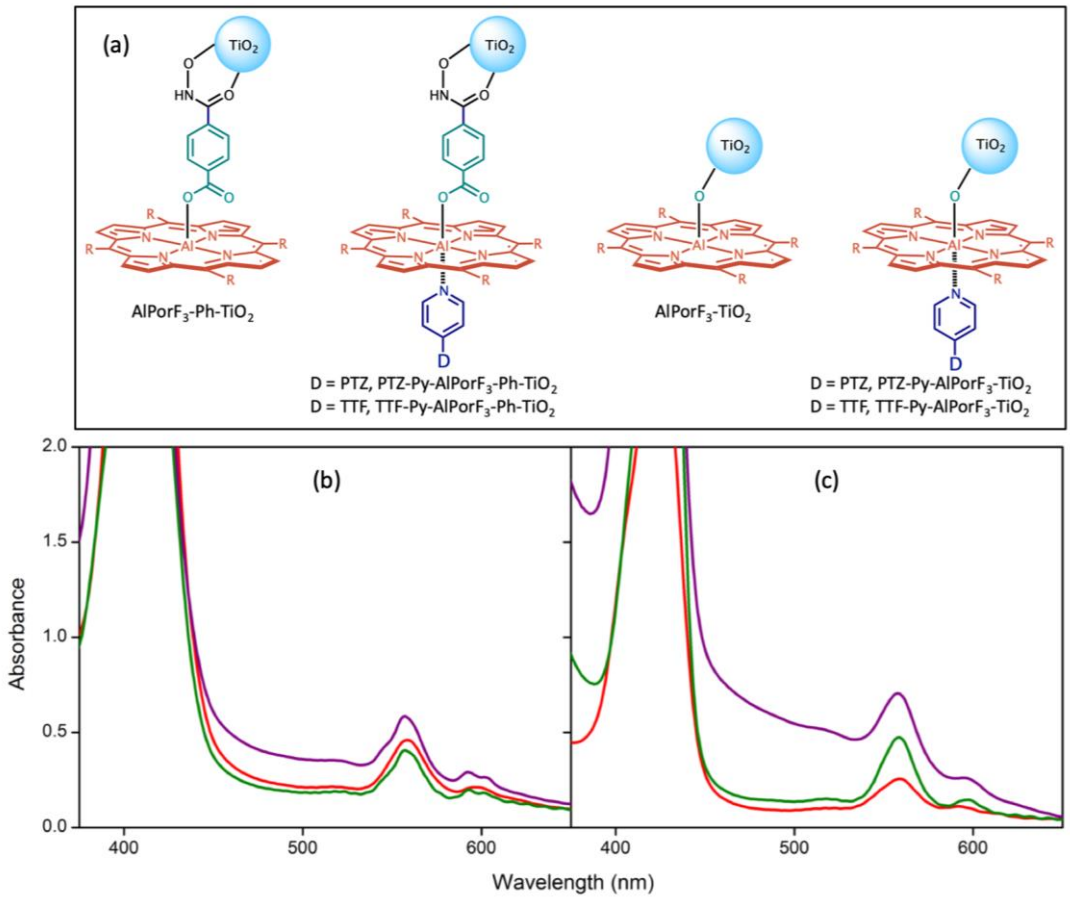

Figure 2. (a) Surface bound multi-modular photoanodes. Absorption spectra of investigated photoanodes: (b) $AlPorF_3$–TiO_2 (red), PTZ–Py–$AlPorF_3$–TiO_2 (green) and TTF–Py–$AlPorF_3$–TiO_2 (purple), and (c) $AlPorF_3$–Ph-TiO_2 (red), PTZ–Py–$AlPorF_3$-Ph–TiO_2 (green) and TTF–Py–$AlPorF_3$-Ph–TiO_2 (purple).

ARTICLE

semiconductor surface. The Lewis acid-base interactions between pyridine of PTZ-Py (or TTF-Py) and Al centre of $AlPorF_3$ were then exploited to construct the PTZ-Py-$AlPorF_3$-TiO_2, TTF-Py-$AlPorF_3$-TiO_2, PTZ-Py-$AlPorF_3$-Ph-TiO_2, and TTF-Py-$AlPorF_3$-Ph-TiO_2 photoanodes, and are show in Figure 4 & 5 insets. One of the differences between the formerly reported photoanodes and in this work is the choice of electron donor. Earlier, we used N,N-Bis(p-anisole)aminopyridine (BAA-Py) as an electron donor.[21] However, the driving force for the hole shift from $AlPorF_3^{\bullet+}$ to BAA was very small. In order to increase the driving force, we have selected electron rich phenothiazine (PTZ-Py) and tetrathiafulvalene (TTF-Py) derivatives in this work. The electron donating ability follows the increasing order of BBA < PTZ < TTF. The substitution of fluorine atoms on the meso phenyl units lower the energy of the excited singlet state making it well poised for injection of electrons into the conduction band of TiO_2 as well as the photo-oxidation of PTZ-Py/TTF-Py.

The investigated photoanodes were fabricated by established methods and are shown in Figure 2a.[21] Briefly, the $AlPorF_3$ was attached chemically to a thin film of transparent TiO_2 nanoparticles on a fused silica microscope slide via phenyl and ether bridges, viz., $AlPorF_3$–Ph–TiO_2 and $AlPorF_3$-TiO_2, respectively. The resulting photoanodes were coordinated with the pyridine-appended donor (TTF–Py or PTZ-Py) by soaking the anodes in a donor solution to produce Donor-Py-$AlPorF_3$-Ph-TiO_2 and Donor-Py-$AlPorF_3$-TiO_2 multi-modular photoanodes. The UV–visible absorption spectra of the resulting constructs are shown in Figure 2b&c. The absorption profiles consist of Soret and Q-bands which is a typical of aluminium(III) porphyrin derivatives. The broadening of the absorption bands suggest that the electronic structure of $AlPorF_3$ is perturbed by the binding as well as the solid-state nature of the sample

4.3 Energetics. The redox potentials of $AlPorF_3$-Ph-HMAH, $AlPorF_3$-Ph, TTF-Py were adopted from our previous papers[21, 28] and summarized in Table 1. The oxidation potential of the PTZ-Py was recorded in CH_2Cl_2 are shown in Figure S3. The difference between the first oxidation potential of the donor and the first reduction potential of the acceptor corresponds to the HOMO–LUMO gap and is the energy of the charge-separated state (E_{CS}), as well as the free-energy changes for charge separation (ΔG_{CS}), are given by Equations (2) and (3):[40]

$$E_{CS} = E^{ox}_{1/2}(Donor) - E^{red}_{1/2}(Acceptor) + G_S \quad (2)$$

$$\Delta G_{CS} = E_{CS} - E_{0\text{-}0} \quad (3)$$

where $E_{0–0}$ is the singlet-state energy of $AlPorF_3$ (2.14 eV), estimated from the blue edge of the fluorescence spectrum at 579 nm. G_S is the ion-pair stabilization and incorporates both the solvent-dependent Coulomb energy change upon ion-pair formation or recombination and the free energy of solvation of the ions [Eq. (4)]:

$$G_S = \frac{-e^2}{4\pi\varepsilon_S\varepsilon_0 R_{D-A}} \quad (4)$$

The centre-to-centre distance ($R_{D\text{-}A}$ = 9.43 and 8.62 Å for TTF-Py-$AlPorF_3$-Ph and PTZ-Py-$AlPorF_3$-Ph, respectively) between donor and acceptor was estimated from Avogadro calculations.[41] ε_S (= 9.1) is the dielectric constant of the CH_2Cl_2, used for the photophysical studies. G_S values of –0.17 for $TTF^{\bullet+}$-$AlPorF_3^{\bullet-}$; –0.18 for $PTZ^{\bullet+}$-$AlPorF_3^{\bullet-}$ are obtained. Together with the optical and redox data the energy level diagrams for the self-assembled dyads (in CH_2Cl_2, Figure 3a) were constructed. It appears that the photoinduced electron transfer from TTF to $^1AlPorF_3$* is exergonic in the investigated solvents for the dyad PTZ-Py-$AlPorF_3$-Ph. Analogous trends were observed for the dyad TTF-Py-$AlPorF_3$-Ph in CH_2Cl_2, that is, the formation of $TTF^{\bullet+}$-$AlPorF_3^{\bullet-}$ charge-separated state is found to be exothermic.

Figure 3b summarizes the energy levels of the investigated compounds on the TiO_2 surface. The energy levels of $AlPorF_3$ and TiO_2 are adopted from our previous paper.[21] The oxidation potentials of PTZ (1.12 V vs NHE) and TTF (0.72 V vs NHE) are derived using the solution state electrochemistry data.[28] As shown in Figure 3b, the HOMO of the secondary electron donor (PTZ or TTF) is higher in energy compared to the HOMO of the $AlPorF_3$, suggesting that the reductive electron transfer is feasible from the secondary donor to $AlPorF_3$ unit. Based on the energy diagram, upon excitation of the $AlPorF_3$, two sequential processes are envisioned in newly constructed photoanodes: (i) an electrons injection from $^1AlPorF_3$* into the conduction band of TiO_2 and (ii) hole shift from oxidized $AlPorF_3$ (viz., $AlPorF_3^{\bullet+}$) to PTZ (or TTF) unit. For comparison purpose, Figure 3b also depicts the energy levels of BAA-Py[21] and the H_2O oxidation with respective to the PTZ-Py and TTF-Py units. The water oxidation ability of the photoanodes decrease from BAA → PTZ → TTF. However, this is not a subject of the study in the current work.

ARTICLE

Table 1. Optical and redox data of investigated compounds in CH_2Cl_2.

Sample	Potential (*vs* SCE)[a]		Absorption λ_{max}, nm (log ε)
	Oxidation	Reduction	
$AlPorF_3$-Ph-HMAH[21]	1.07, 1.38	−1.04, −1.47	593 (3.53), 554 (4.32), 418 (5.59)
$AlPorF_3$-Ph[21]	1.04	−1.03, −1.43	593 (3.46), 554 (4.30), 418 (5.56)
TTF-Py[28]	0.48, 0.83	-	295 (4.20), 275 (4.22)
PTZ-Py[27]	0.88	-	256 (4.61), 314 (3.65)
BAA-Py[21]	1.00	-	295 (4.20), 275 (4.22)

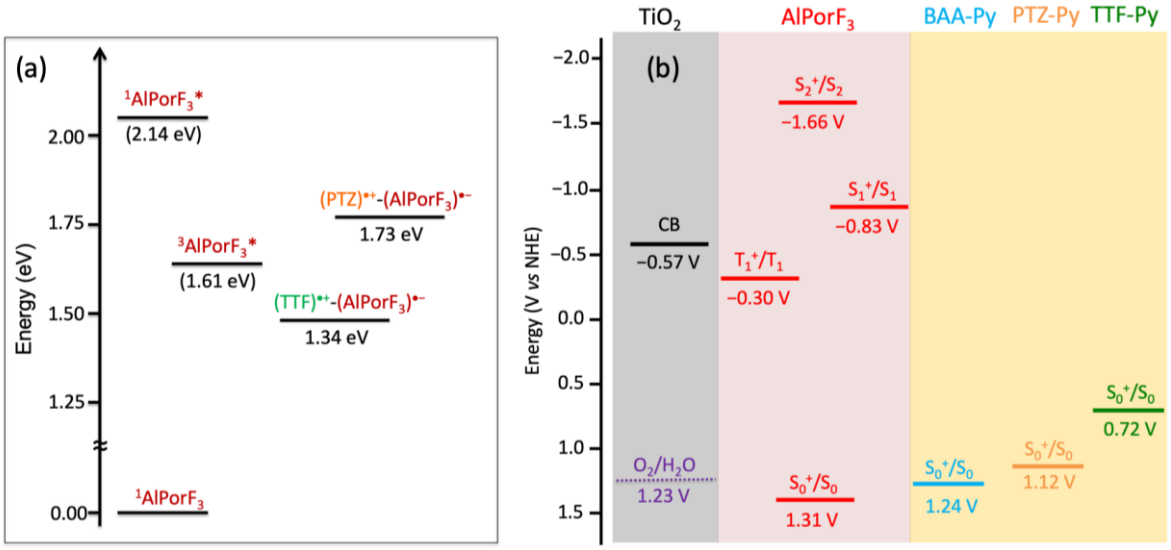

Figure 3. Energy level diagram of redox-active units $AlPorF_3$, PTZ, TTF and TiO_2: (a) in CH_2Cl_2, (b) on TiO_2 surface. CB = conduction band, S = singlet state, T = triplet state. NHE = SCE + 0.24 V. For the comparison purpose the oxidation potentials of BAA and H_2O are depicted in (b).

4.4 Fluorescence titrations. The steady-state fluorescence spectra of investigated compounds are reported elsewhere.[21] The fluorescence spectra of the $AlPorF_3$-Ph-HMAH and $AlPorF_3$-Ph are very similar in spectral shapes as well as fluorescence intensities revealing that the electronic structure of the $AlPorF_3$ is not perturbed by the axial phenyl unit. Figure 1b show fluorescence titrations of the $AlPorF_3$-Ph in the presence of increasing amounts of PTZ-Py. The titrations were carried out in CH_2Cl_2 and the samples were excited at the isosbestic point 550 nm, which is obtained from corresponding absorption titrations, see Figure 1a. Upon addition of PTZ-Py, a red shift of the fluorescence bands from 599 and 645 nm to 607 and 660 nm, respectively, with isosbestic points at 597, 624 and 651 nm were observed. The relative fluorescence intensity ratios at 607/599 and 660/645 nm were found to be 1.87 and 1.07, respectively. To understand the trends, these results were compared with titrations of $AlPorF_3$-Ph with Py (without PTZ moiety), and are adopted from elsewhere.[21] Similar red shift was revealed in the $AlPorF_3$ emission bands upon addition of Py. However, the relative intensity ratios at 607/593 and 660/643 nm were found to be 2.85 and 1.23, respectively. Based on the relative intensities, it was clear that there is a moderate

quenching in the $AlPorF_3$ fluorescence during the titration of $AlPorF_3$-Ph vs PTZ-Py. Hence, we conclude that the red shift is the result of the coordination of Py to $AlPorF_3$ unit whereas the fluorescence quenching is due an intramolecular electron transfer from PTZ to $^1(AlPorF_3)^*$ to yield $(PTZ)^{\bullet+}$-$(AlPorF_3)^{\bullet-}$. The corresponding ΔG_{CS} for this process is estimated to be −0.41 eV. In order to evaluate the photoinduced process between $AlPorF_3$ and TTF the fluorescence titrations were performed, see Figure 1d. Upon addition of TTF-Py to the $AlPorF_3$-Ph solution, strong fluorescence quenching was revealed due to the formation of coordination complex TTF-Py-$AlPorF_3$-Ph. Moreover, fluorescence bands red shifted from 597 and 645 nm to 605 and 653 nm, respectively. Based on the energy level diagram, the observed quenching is assigned to electron transfer from TTF to $^1AlPorF_3$* as the ΔG_{CS} for this process is estimated to be −0.80 eV.

4.5 Transient Absorption Spectroscopic Studies. Finally, femtosecond transient spectral studies were performed to secure evidence of (i) charge injection from the surface immobilized $^1AlPorF_3$* to the conduction band of TiO_2, and (ii) hole migration from the axially coordinated electron donors, phenothiazine and tetrathiafulvalene, to $AlPorF_3^{\bullet+}$ resulting in slower charge recombination processes. Figure S4 shows the femtosecond transient absorption spectra of $AlPorF_3$-OH and $AlPorF_3$-Ph-HMA in o-dichlorobenzene (o-DCB). In agreement with the earlier discussed pristine $AlPorF_3$,[21] the spectral features of both $AlPorF_3$-OH and $AlPorF_3$-Ph-HMAH were almost the same. In the case of $AlPorF_3$-OH, the instantaneously formed $^1AlPorF_3$* revealed positive peaks at 455, 580, 616, and 1225 nm and negative peaks at 552, 592, and 654 nm. The positive peaks were attributed to transitions originating from the singlet excited state of $AlPorF_3$ while the 552 nm negative peak was attributed to ground state bleach while the 592 and 654 nm peaks were attributed to stimulated emission. Similar features were observed for $AlPorF_3$-Ph-HMAH also. The decay of the positive peaks lasted over 3 ns, as shown for the near-IR peak monitored at 1225 nm, consistent with the relatively long fluorescence lifetime of $AlPorF_3$-OH and $AlPorF_3$-Ph-HMAH being 3.30 and 3.47 ns, respectively.

In order to help interpret the transient spectral data related to charge injection and recombination, spectroelectrochemical studies were performed on $AlPorF_3$ and the two electron donors, as shown in Figure S5. To generate the spectrum of the one-electron oxidized products, an applied voltage past 120 mV of the first oxidation potential was applied in each case on a transparent working electrode, and spectra were recorded during the course of electrolysis in a thin-layer optical cell. The one-electron oxidized product of $AlPorF_3$, viz., $AlPorF_3^{\bullet+}$ revealed new peaks at 595 and 690 nm while $PTZ^{\bullet+}$-Py had a peak at 445 nm with much lower intensity compared to the neutral compound. The one-electron oxidized product of TTF-Py, viz., $TTF^{\bullet+}$-Py revealed two peaks at 450 and 610 nm.

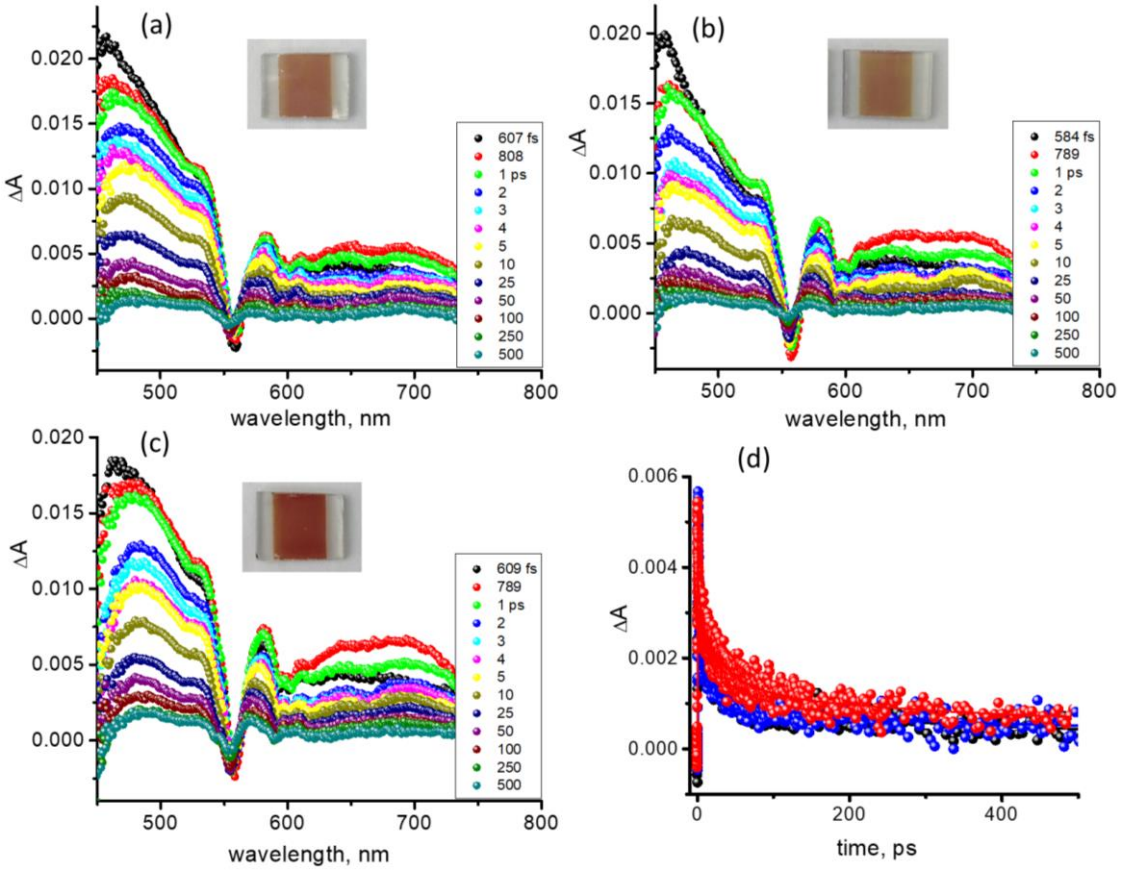

Figure 4. Femtosecond transient spectra at the indicated delay times of (a) $AlPorF_3$-TiO_2, (b) PTZ-Py-$AlPorF_3$-TiO_2, and (c) TTF-Py-$AlPorF_3$-TiO_2 photoanodes (see figure inset for pictures of the photoanodes). The decay profile of the 692 nm peak corresponding to $AlPorF_3^{\bullet+}$ is shown in (d) $AlPorF_3$-TiO_2 (black), PTZ-Py-$AlPorF_3$-TiO_2 (blue), and TTF-Py-$AlPorF_3$-TiO_2 (red).

ARTICLE

Figures 4a and 5a, respectively, show transient absorption spectra of $AlPorF_3$-TiO_2 and $AlPorF_3$-Ph-TiO_2, see Figure 2a for structures. As predicted for the charge injection process, in both cases, the deactivation of transient peaks originated from $^1AlPorF_3$* were rapid. In addition, a new broad signal in the 600-750 nm that was not present in the solution transient spectra of $AlPorF_3$-OH and $AlPorF_3$-Ph-HMAH was observed (see Figure S6 in ESI for rise components). The peak position was in agreement with that of $AlPorF_3^{\bullet+}$, suggesting that both $AlPorF_3$ are indeed involved in charge injection from the singlet excited state to the conduction band of TiO_2.[21] The reduced TiO_2 is expected to have a signal in the mid-IR[42] and THz[43, 44] regions beyond the monitoring wavelength window of our spectrometer. In order to evaluate the kinetics, the time profile of $AlPorF_3^{\bullet+}$ at 692 nm was monitored. The time constants for the decay (see Figures 4d and 5d for decay profiles) were found to be 67 ps for $AlPorF_3$-TiO_2, and 100 ps for $AlPorF_3$-Ph-TiO_2. The higher time constant (slower charge recombination) in the case of $AlPorF_3$-Ph-TiO_2 is understandable due to the bridging Ph-HMAH separating the $AlPorF_3$ and TiO_2 (see Figure 2 for structures) compared to the direct binding in the former case, viz., $AlPorF_3$-TiO_2.

As discussed earlier, assembling a secondary electron donor through the metal-ligand axial coordination would neutralize the $AlPorF_3^{\bullet+}$ by a hole transfer mechanism, thus, distantly separating the cationic and anionic species, $D^{\bullet+}$-$AlPorF_3$-$TiO_2^{\bullet-}$ (D = secondary donor held via axial ligation) of the initial electron transfer product. The overall effect would be slowing down the charge recombination process and lowering the overall lifetime of the $AlPorF_3^{\bullet+}$ species. To verify these predictions, transient spectral measurements were repeated in the presence of axially bound secondary electron donors. First, in order to verify that the axial pyridine used in coordination had no effect on photodynamics, pyridine was coordinated to

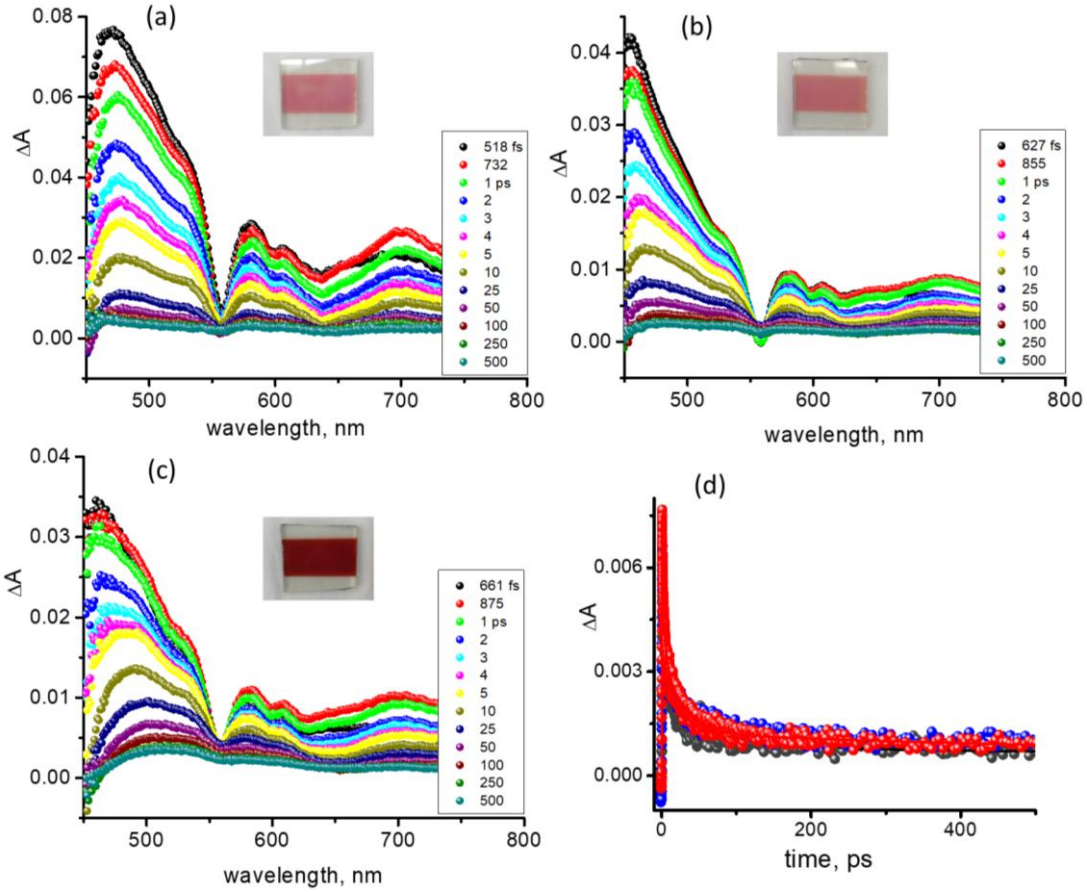

Figure 5. Femtosecond transient spectra at the indicated delay times of (a) $AlPorF_3$-Ph-TiO_2, (b) PTZ-Py-$AlPorF_3$-Ph-TiO_2, and (c) TTF-Py-$AlPorF_3$-Ph-TiO_2 photoanodes (see figure inset for pictures of the photoanodes). The decay profile of the 692 nm peak corresponding to $AlPorF_3^{\bullet+}$ is shown in (d) $AlPorF_3$-Ph-TiO_2 (black), PTZ-Py-$AlPorF_3$-Ph-TiO_2 (blue), and TTF-Py-$AlPorF_3$-Ph-TiO_2 (red).

ARTICLE

$AlPorF_3$ and the transient spectra were measured. The time constants for the 692 nm peak corresponding to $AlPorF_3^{\bullet+}$ were found to be 66 ps for Py-$AlPorF_3$-TiO_2, and 113 ps for Py-$AlPorF_3$-Ph-TiO_2, not significantly different from that without coordinated pyridine. These results indicate that the coordinated pyridine is not directly involved in a hole transfer process.

Figures 4b and c, respectively, show transient absorption spectra at the indicated delay times for PTZ-Py-$AlPorF_3$-TiO_2, and TTF-Py-$AlPorF_3$-TiO_2 while Figures 5b and c, respectively, show those for PTZ-Py-$AlPorF_3$-Ph-TiO_2 and TTF-Py-$AlPorF_3$-Ph-TiO_2 photoanodes. The spectral features were very close to those observed without axial secondary donors, however, with subtle changes. Generally, the intensity corresponding to $AlPorF_3^{\bullet+}$ peak in the 600-750 nm range was smaller than that observed in the absence of secondary electron donors (see spectra after 3 ps). This could be rationalized based on the hole transfer mechanism where $AlPorF_3^{\bullet+}$ is neutralized by the secondary donors. The earlier discussed spectroelectrochemical results revealed $PTZ^{\bullet+}$-Py peak at 445 nm and $TTF^{\bullet+}$-Py peaks at 450 and 610 nm. The spectra recorded for the axial donor bound systems, revealed spectral broadening in the 450 nm range suggesting contributions from the $PTZ^{\bullet+}$-Py and $TTF^{\bullet+}$-Py species, although it was difficult to isolate the signal due to strong transitions originating from $^1AlPorF_3$* in the spectral range. The net effect of these events, that is, hole transfer promoted slower charge recombination, could be visualized by the decay kinetics of the 692 nm peak corresponding to $AlPorF_3^{\bullet+}$, as shown in Figures 4d and 5d. The time constants for the decay process was found to be 40 ps for PTZ-Py-$AlPorF_3$-TiO_2, 28 ps for TTF-Py-$AlPorF_3$-TiO_2, 60 ps for PTZ-Py-$AlPorF_3$-Ph-TiO_2 and 42 ps for TTF-Py-$AlPorF_3$-Ph-TiO_2 photoanodes. That is, faster recovery of $AlPorF_3^{\bullet+}$ due to contributions of electron transfer from the secondary donor to $AlPorF_3^{\bullet+}$, thus lowering the overall lifetime of the latter species was witnessed. Additionally, this effect was better defined for photoanodes having TTF as a secondary donor which could be rationalized due to facile oxidation of TTF over PTZ. Also, the recombination kinetics was slower for photoanodes with Ph-HMAH bridging rather than oxygen bridging due to overall donor-acceptor distances. In summary, the role of secondary electron donors, PTZ and TTF in slowing the charge recombination process due to hole transfer mechanism is borne out from this study. It is important to note that due to the ultrafast electron injection process, it is most likely that the electron injection takes place in a first place from $^1AlPorF_3$* to TiO_2 followed by hole transfer from $AlPorF_3^{\bullet+}$ to secondary electron donor.

Table 2 summarizes rise and decay time constants of $AlPorF_3^{\bullet+}$ and the rate constants for charge injection and decay for the presently investigated systems along with systems derived by assembling photoanodes by N,N-bis(p-anisole)aminopyridine (abbreviated as BAA-Py),[21] another second electron donor of this class. An examination of data from the table reveals the following: (i) the charge injection kinetics are very fast approaching the detection limit of the instrument, and the presence of second electron donor further accelerates such a process. (ii) Decay kinetics of $AlPorF_3^{\bullet+}$ is accelerated by the secondary electron donors due to the hole migration process lowering the overall lifetime of the radical cation species. (iii) There is a free-energy correlation between k_D and the secondary electron donor, that is, k_D follows the trend TTF (E_{ox} = 0.48 V) > PTZ (E_{ox} = 0.88 V) > BAA (E_{ox} = 1.24 V). As shown in the energy level diagram the driving force for the hole transfer process increases from BAA to TTF. (iv) Distance between $AlPorF_3$ and TiO_2 also seem to play an important role, that is, both k_f and k_D were faster for $AlPorF_3$-TiO_2 photoanodes compared to $AlPorF_3$-Ph-TiO_2 photoanodes due to close association of the sensitizer to the TiO_2 surface in the former case.

Table 2. The evaluated time constants, and the rates of formation (k_f), and decay (k_D) of $AlPorF_3^{\bullet+}$ on the modified TiO_2 surface (estimated error ±5%)

Photoanode	Time constants		Rate constants		Ref
	τ_f, ps	τ_D, ps	k_f, s^{-1}	k_D, s^{-1}	
$AlPorF_3$-TiO_2	1.7	73.8	6.0×10^{11}	13.5×10^9	[21]
BAA-Py-$AlPorF_3$-TiO_2	0.7	55.8	14.5×10^{11}	17.9×10^9	[21]
PTZ-Py-$AlPorF_3$-TiO_2	0.7	40.0	14.5×10^{11}	25.0×10^9	tw
TTF-Py-$AlPorF_3$-TiO_2	0.4	28.0	25.0×10^{11}	35.7×10^9	tw
$AlPorF_3$-Ph-TiO_2	2.1	100.0	4.9×10^{11}	9.9×10^9	[21]
BAA-Py-$AlPorF_3$-Ph-TiO_2	1.8	81.0	5.5×10^{11}	12.3×10^9	[21]
PTZ-Py-$AlPorF_3$-Ph-TiO_2	2.2	60.0	4.5×10^{11}	16.6×10^9	tw
TTF-Py-$AlPorF_3$-Ph-TiO_2	1.9	42.0	5.2×10^{11}	30.7×10^9	tw

tw = this work

ARTICLE

(v) The k_D value is independent of the Ph-spacer because it is depending on the electron donating ability of the secondary donor. Whereas, k_f values are dependent on Ph because this process is between $AlPorF_3$ and TiO_2 moieties, where distance play a role on the rates. (vi) The k_f values accelerate to some extent for $AlPorF_3$-TiO_2 than $AlPorF_3$-Ph-TiO_2 in the presence of secondary electron donor. The acceleration of k_f in Donor-$AlPorF_3$-TiO_2 can be explained by the coordination of secondary electron donor. As discussed in section 4.1, upon coordination of a secondary donor the Al centre is pulled into the porphyrin plane, which brings the porphyrin bit closer to the TiO_2 surface. As a result, the distance between $AlPorF_3$ and TiO_2 surface slightly decreases. This, in principle, could increase the orbital overlap between $AlPorF_3$ and TiO_2, and may accelerate the electron injection (increase in k_f) process in the case of D-$AlPorF_3$-TiO_2. The same is expected for D-$AlPorF_3$-Ph-TiO_2, however, due to Ph spacer the orbital overlap would be insignificant or not feasible. Therefore, the k_f acceleration is not pronounced in D-$AlPorF_3$-Ph-TiO_2 systems. Additional factors that contribute to this observation may also include subtle oxidation potential changes of $AlPorF_3$ upon binding to nitrogenous ligand. (vii) Using the data in Table 2 it is possible to estimate the rate of electron donation by each of the donors by subtracting the rate observed without the donor from the rate observed with the donor. The calculated rates were found to be (x 10^9 s^{-1}): 4.4, 11.5 and 21.9 for BAA-Py-$AlPorF_3$-TiO_2, PTZ-Py-$AlPorF_3$-TiO_2 and TTF-Py-$AlPorF_3$-TiO_2, respectively; 2.4, 6.7 and 20.8 for BAA-Py-$AlPorF_3$-Ph-TiO_2, PTZ-Py-$AlPorF_3$-Ph-TiO_2 and TTF-Py-$AlPorF_3$-Ph-TiO_2, respectively. The calculated rates, although an approximation due to the time scale with which they occur, indicate that the donation rates are more or less independent of the linker between the porphyrin and the TiO_2 surface.

5. Conclusions.

We have shown that the aluminium(III) porphyrins are effective photosensitizers for photoanodes when covalently bound to TiO_2 surfaces. The results presented here show that the unique properties of aluminium(III) porphyrin can be exploited for the construction of self-assembled photoanodes on TiO_2 surface. In these photoanodes, AlPor is covalently linked to the TiO_2 surface, while the Donor−Py is coordinated to the Al centre through Lewis acid−base interactions. This strategy provides a vertical arrangement of chromophore and electron donor on the metal oxide surface. Using the steady-state and transient spectroscopy we show that, upon photoexcitation with visible light, ultrafast electron injection takes place from $AlPorF_3$ into the conduction band of TiO_2, and this is followed by oxidation of the secondary electron donor PTZ or TTF. The later process made possible due to the formation of $AlPorF_3^{\bullet+}$, which holds enough anodic potential to oxidize the coordinated secondary electron donor. Ultimately, our self-assembly strategy provides a way to attach a water oxidation catalyst, by replacing the secondary electron donor, to a photosensitizer on the metal oxide surface. Studies in this direction are in progress.

Acknowledgements. This work was supported by startup grants from the University of Minnesota Duluth, to PPK, and by the National Science Foundation (Grant No. 1401188) to FD.

Conflicts of interest

There are no conflicts to declare.

References

1. L. Alibabaei, M. K. Brennaman, M. R. Norris, B. Kalanyan, W. J. Song, M. D. Losego, J. J. Concepcion, R. A. Binstead, G. N. Parsons and T. J. Meyer, *Proc. Natl. Acad. Sci. U. S. A.*, 2013, **110**, 20008-20013.
2. C. A. Bignozzi, R. Argazzi, R. Boaretto, E. Busatto, S. Carli, F. Ronconi and S. Caramori, *Coordination Chemistry Reviews*, 2013, **257**, 1472-1492.
3. Y. Gao, X. Ding, J. H. Liu, L. Wang, Z. K. Lu, L. Li and L. C. Sun, *J. Am. Chem. Soc.*, 2013, **135**, 4219-4222.
4. M. Gratzel, *Acc Chem. Res.*, 2009, **42**, 1788-1798.
5. B. G. Kim, K. Chung and J. Kim, *Chem-Eur J*, 2013, **19**, 5220-5230.
6. T. J. Meyer, L. Alibabaei, M. K. Brennaman, M. R. Norris, B. Kalanyan, W. J. Song, M. D. Losego, J. J. Concepcion, R. A. Binstead and G. N. Parsons, *Abstr. Pap. Am. Chem. Soc.*, 2014, **247**.
7. I. Obraztsov, W. Kutner and F. D'Souza, *Solar RRL*, 2017, **1**, n/a-n/a.
8. K. J. Young, L. A. Martini, R. L. Milot, R. C. Snoeberger, V. S. Batista, C. A. Schmuttenmaer, R. H. Crabtree and G. W. Brudvig, *Coordination Chemistry Reviews*, 2012, **256**, 2503-2520.
9. W. J. Youngblood, S. H. A. Lee, Y. Kobayashi, E. A. Hernandez-Pagan, P. G. Hoertz, T. A. Moore, A. L. Moore, D. Gust and T. E. Mallouk, *J. Am. Chem. Soc.*, 2009, **131**, 926-+.
10. Y. X. Zhao, J. R. Swierk, J. D. Megiatto, B. Sherman, W. J. Youngblood, D. D. Qin, D. M. Lentz, A. L. Moore, T. A. Moore, D. Gust and T. E. Mallouk, *Proc. Natl. Acad. Sci. U. S. A.*, 2012, **109**, 15612-15616.
11. J. Barber and B. Andersson, *Nature*, 1994, **370**, 31-34.
12. J. Deisenhofer, Norris, J. R., ed., *The Photosynthetic Reaction Center*, Academic Press, San Diego, CA, 1993.
13. P. Fromme, *Curr. Opin. Struct. Biol.*, 1996, **6**, 473-484.
14. N. Krauss, W. D. Schubert, O. Klukas, P. Fromme, H. T. Witt and W. Saenger, *Nat. Struct. Biol.*, 1996, **3**, 965-973.

15. J. M. Gardner, M. Beyler, M. Karnahl, S. Tschierlei, S. Ott and L. Hammarstrom, *J. Am. Chem. Soc.*, 2012, **134**, 19322-19325.
16. L. A. Martini, G. F. Moore, R. L. Milot, L. Z. Cai, S. W. Sheehan, C. A. Schmuttenmaer, G. W. Brudvig and R. H. Crabtree, *Journal of Physical Chemistry C*, 2013, **117**, 14526-14533.
17. G. F. Moore, J. D. Blakemore, R. L. Milot, J. F. Hull, H. E. Song, L. Cai, C. A. Schmuttenmaer, R. H. Crabtree and G. W. Brudvig, *Energy Environ. Sci.*, 2011, **4**, 2389-2392.
18. G. F. Moore, S. J. Konezny, H. E. Song, R. L. Milot, J. D. Blakemore, M. L. Lee, V. S. Batista, C. A. Schmuttenmaer, R. H. Crabtree and G. W. Brudvig, *Journal of Physical Chemistry C*, 2012, **116**, 4892-4902.
19. R. L. Milot and C. A. Schmuttenmaer, *Acc Chem. Res.*, 2015, **48**, 1423-1431.
20. P. K. Poddutoori, J. M. Thomsen, R. L. Milot, S. W. Sheehan, C. F. A. Negre, V. K. R. Garapati, C. A. Schmuttenmaer, V. S. Batista, G. W. Brudvig and A. van der Est, *J. Mater. Chem. A*, 2015, **3**, 3868-3879.
21. G. N. Lim, S. Hedstrom, K. A. Jung, P. A. D. Smith, V. S. Batista, F. D'Souza, A. van der Est and P. K. Poddutoori, *Journal of Physical Chemistry C*, 2017, **121**, 14484-14497.
22. K. L. Materna, J. Jiang, K. P. Regan, C. A. Schmuttenmaer, R. H. Crabtree and G. W. Brudvig, *ChemSusChem*, 2017, **10**, 4526-4534.
23. P. K. Poddutoori, G. N. Lim, M. Pilkington, F. D'Souza and A. van der Est, *Inorganic Chemistry*, 2016, **55**, 11383-11395.
24. P. K. Poddutoori, L. P. Bregles, G. N. Lim, P. Boland, R. G. Kerr and F. D'Souza, *Inorganic Chemistry*, 2015, **54**, 8482-8494.
25. P. K. Poddutoori, G. N. Lim, A. S. D. Sandanayaka, P. A. Karr, O. Ito, F. D'Souza, M. Pilkington and A. van der Est, *Nanoscale*, 2015, **7**, 12151-12165.
26. P. K. Poddutoori, G. N. Lim, S. Vassiliev and F. D'Souza, *Phys. Chem. Chem. Phys.*, 2015, **17**, 26346-26358.
27. P. K. Poddutoori, A. S. D. Sandanayaka, N. Zarrabi, T. Hasobe, O. Ito and A. van der Est, *J Phys Chem A*, 2011, **115**, 709-717.
28. P. K. Poddutoori, N. Zarrabi, A. G. Moiseev, R. Gumbau-Brisa, S. Vassiliev and A. van der Est, *Chem-Eur J*, 2013, **19**, 3148-3161.
29. N. Zarrabi, C. Agatemor, G. N. Lim, A. J. Matula, B. J. Bayard, V. S. Batista, F. D'Souza and P. K. Poddutoori, *Journal of Physical Chemistry C*, 2019, **123**, 131-143.
30. N. Zarrabi, C. O. Obondi, G. N. Lim, S. Seetharaman, B. G. Boe, F. D'Souza and P. K. Poddutoori, *Nanoscale*, 2018, **10**, 20723-20739.
31. P. K. Poddutoori, P. Poddutoori, B. G. Maiya, T. K. Prasad, Y. E. Kandrashkin, S. Vasil'ev, D. Bruce and A. van der Est, *Inorganic Chemistry*, 2008, **47**, 7512-7522.
32. P. K. Poddutoori, Y. E. Kandrashkin and A. van der Est, *Zeitschrift Fur Physikalische Chemie-International Journal of Research in Physical Chemistry & Chemical Physics*, 2017, **231**, 293-310.
33. P. K. Poddutoori, A. S. D. Sandanayaka, T. Hasobe, O. Ito and A. van der Est, *J. Phys. Chem. B*, 2010, **114**, 14348-14357.
34. A. Amati, P. Cavigli, A. Kahnt, M. T. Indelli and E. Iengo, *J Phys Chem A*, 2017, **121**, 4242-4252.
35. A. Bagaki, H. B. Gobeze, G. Charalambidis, A. Charisiadis, C. Stangel, V. Nikolaou, A. Stergiou, N. Tagmatarchis, F. D'Souza and A. G. Coutsolelos, *Inorganic Chemistry*, 2017, **56**, 10268-10280.
36. E. Iengo, P. Cavigli, M. Gamberoni and M. T. Indelli, *European Journal of Inorganic Chemistry*, 2014, **2014**, 337-344.
37. E. Lengo, G. D. Pantos, J. K. M. Sanders, M. Orlandi, C. Chiorboli, S. Fracasso and F. Scandola, *Chemical Science*, 2011, **2**, 676-685.
38. M. Natali, R. Argazzi, C. Chiorboli, E. Iengo and F. Scandola, *Chem-Eur J*, 2013, **19**, 9261-9271.
39. P. Thordarson, *Chem. Soc. Rev.*, 2011, **40**, 1305-1323.
40. D. Rehm and A. Weller, *Israel Journal of Chemistry*, 1970, **8**, 259-&.
41. W. A. de Jong, A. M. Walker and M. D. Hanwell, *Journal of Cheminformatics*, 2013, **5**.
42. H. N. Ghosh, J. B. Asbury and T. Q. Lian, *J. Phys. Chem. B*, 1998, **102**, 6482-6486.
43. E. Hendry, F. Wang, J. Shan, T. F. Heinz and M. Bonn, *Physical Review B*, 2004, **69**.
44. C. Richter and C. A. Schmuttenmaer, *Nature Nanotechnology*, 2010, **5**, 769-772.

Table of Contents Entry:

Surface Anchored Self-Assembled Reaction Center Mimics as Photoanodes Consisting of a Secondary Electron Donor, Aluminum(III) Porphyrin and TiO_2 Semiconductor

Niloofar Zarrabi,[a] Gary N. Lim,[b] Brandon J. Bayard,[a] Francis D'Souza,[,b] Prashanth K. Poddutoori *[,a]*

Vertically assembled photoanodes, consists of aluminum(III) porphyrin, electron donor, and semiconductor TiO_2, have been fabricated and their photophysical properties investigated.